Electrohydraulic effects on the modelling of a vehicle active suspension

J Watton, K. M. Holford and P Surawattanawan

Proceedings of the Institution of Mechanical Engineers, Part D: Journal of Automobile Engineering 2001 215: 1077
DOI: 10.1243/0954407011528635

Electrohydraulic effects on the modelling of a vehicle active suspension

J Watton*, K M Holford and **P Surawattanawan**
Mechanical Engineering and Energy Studies Division, Cardiff School of Engineering, Cardiff University, Wales, UK

Abstract: A car suspension incorporating a Lotus actuator and a TVR suspension/wheel unit is studied both experimentally and analytically. An emphasis is placed on hydraulic modelling using a series of transfer functions linking the hydraulic and suspension components. This is significantly aided by the use of a Moog 2000 programmable servo controller (PSC) to equalize the extending and retracting flow gains of the servovalve in the Lotus actuator control loop, justifying the use of combined extending and retracting transient data for parameter identification. This then allows the system equations to be developed using linear state-space theory, and a suitable form is proposed for further design studies. It is shown that the hydraulic components significantly contribute to the system dynamics and hence cannot be neglected when control schemes are formulated. In particular, the significance of hydraulic bulk modulus on dynamic performance is evaluated, and the importance of accurately determining all components of velocity-type damping is highlighted.

Keywords: active suspension, modelling, electrohydraulic control

NOTATION

A	actuator cross-sectional area $= 2.46 \times 10^{-4}$ m^2
$\mathbf{A}$	open-loop state-space matrix
B_t	tyre damping $= 4000$ N/m s
B_v	hydraulic cylinder and linkage damping $= 300$ N/m s
$\boldsymbol{B}$	open-loop state-space vector
e	error signal
F	hydraulic force
F_1	LVDT gain $= 57.2$ V/m
F_2	feedback gain $= 1$
G	Moog 2000 program D/A gain $= 6.25 \times 10^{-3}$ mA/PSC no.
$\boldsymbol{G}_d$	open-loop state-space vector
i	servovalve current
i_0	steady state applied servovalve current
I_1, J_1, H_1, F_1, L_1	gain elements of the feedback vector
I_2, J_2, H_2, F_2, L_2	transducer gain elements of the gain matrix
k_f	servovalve flow constant
k_i	linearized servovalve flow constant $= 2.3 \times 10^{-5}$ m^3/s mA
k_o	hydraulic oil stiffness
k_t	tyre stiffness $= 2.8 \times 10^5$ N/m
$\boldsymbol{K}$	state feedback gain vector
$\boldsymbol{K}_1$	state feedback gain vector
$\mathbf{K}_2$	transducer gain matrix
m	wheel and tyre mass (unsprung mass, quarter-car model) $= 40$ kg
M	carbody mass (sprung mass, quarter-car model) $= 240$ kg
N	Moog 2000 program A/D gain $= 1600$ PSC no./V
P	forward gain for two-degree-of-freedom (2 DOF) test $= 0.85$
P_L	load pressure
P_s	supply pressure
P_t	tank return pressure
P_1, P_2	pressures
P_{10}, P_{20}	steady-state pressures
Q_1, Q_2	flowrates
R	forward gain for the single-degree-of-freedom (1 DOF) test $= 0.4$
R_i	cross-line leakage resistance $= 9.8 \times 10^{10}$ N/m^2/m^3 s
V	actuator and hose volume $= 7.13 \times 10^{-5}$ m^3

The MS was received on 23 May 2001 and was accepted after revision for publication on 21 June 2001.
** Corresponding author: Mechanical Engineering and Energy Studies Division, Cardiff School of Engineering, Cardiff University, Queen's Buildings, The Parade, PO Box 685, Cardiff CF2 3TA, Wales, UK.*

$\boldsymbol{x}$	open-loop state vector
z_b	absolute displacement of the carbody
$z_b - z_w$	relative displacement of the carbody and wheel
$(z_b - z_w)_f$	feedback signal of $z_b - z_w$
z_r	absolute displacement of the road disturbance
$z_r - z_w$	relative displacement of the road disturbance and wheel
z_{ref}	reference signal of z_b
z_w	wheel (unsprung mass) absolute displacement
$\dot{z}_b$	carbody (sprung mass) velocity
$\dot{z}_r$	velocity of the road disturbance
$\dot{z}_w$	wheel (unsprung mass) velocity
$\ddot{z}_b$	carbody (sprung mass) acceleration
$\ddot{z}_w$	wheel (unsprung mass) acceleration
α	actuator angle $= 27^\circ$
β_e	effective bulk modulus $= 0.22 \times 10^9$ N/m^2
ω	undamped natural frequencies for the locked actuator condition

1 INTRODUCTION

Development of the Lotus active suspension system was initiated to solve the aerodynamic problems of controlling large down-forces without compromising driver conditions or handling [**1**–**4**]. The Lotus control model, along with skyhook active damping, has formed the basis for most active and semi-active approaches to suspension control. This work is concerned with fully active control utilizing a Lotus actuator controlled by a Moog servovalve, with the objective of obtaining realistic electrohydraulic models for control system design. This has been found necessary from initial tests which showed a great disparity between measurements and conventional modelling of system dynamics. Vehicle suspension systems can take several forms varying from passive to semi-active to fully active, and utilizing a range of gas or oil hydraulic, active or passive, components. Various overviews (e.g. references [**5**] to [**8**]) indicate the scope of the subject and give some insight into system modelling and related control schemes. However, the practical solutions depend upon the bounds of the theory and the control/sensing scheme selected. Many publications tend to neglect hydraulic component modelling, but in some cases a mixture of simulation and experimental testing has shown promise, although detailed comparisons between submodel predictions and measurement are not evident [**9**–**15**].

2 SYSTEM DYNAMICS WITH NO ACTIVE CONTROL

Consider the quarter-car active suspension system shown in Fig. 1. Both road and active actuator are controlled using Moog electrohydraulic servovalves and Moog M2000 programmable servo controllers (PSCs) operating with 2 ms sampling intervals. The TVR suspension and wheel unit is linked at an angle α to the plane of movement of the body mass, which is constrained to move vertically via linear bearings. A load cell is positioned between the actuator body and car body pivot point, and LVDT position transducers together with velocity transducers are appropriately placed to measure road, wheel and body motion. Accelerometers were fixed to the wheel and the body in anticipation of future control performance assessment, but they were not used for this study.

A schematic of the experimental set-up is shown in Fig. 2. Data were collected via a high-speed parallel-channel data acquisition card system to enable further analysis to be undertaken using the MATLAB simulation and signal processing environment.

A vast amount of experimental testing was carried out using both frequency response, via a transfer function analyser with pseudobinary random signal excitation, and transient analysis, via the step response method. General trends in frequency response were clearly identified, but the Bode diagrams were not sufficiently accurate for comparison purposes beyond a frequency of typically 15 Hz, and inadequate to use for parameter identification. Therefore, modelling concepts are presented via the transfer function approach, in keeping with most of the background literature, and experimental parameter identification and validation were achieved using step response testing.

To obtain a feel for the dynamic behaviour, Fig. 3 illustrates the dynamic linear model for the hypothetical situation with the actuator fixed in its central position and with no active control. This is not possible to achieve in practice because of cross-line leakage, which results in the carbody mass moving to its rest position, but serves to illustrate the frequency domain of interest. Therefore, the servovalve spool is assumed to be centred in the absence of an input signal.

Actuator and lines create an oil stiffness contribution, k_o, together with velocity damping generated by oil viscosity effects and also a suspension mechanical friction component to a lesser extent. Oil stiffness is defined with the actuator in its central position and equal length lines, and hence with equal oil volumes on either side. The viscous damping effect is labelled as B_v, and the cross-line leakage may also be considered to be equivalent to velocity damping, B_o, in series with oil stiffness k_o. The wheel tyre has a stiffness k_t together with an assumed velocity damping B_t. The parameter identification work described later, together with direct measurements where

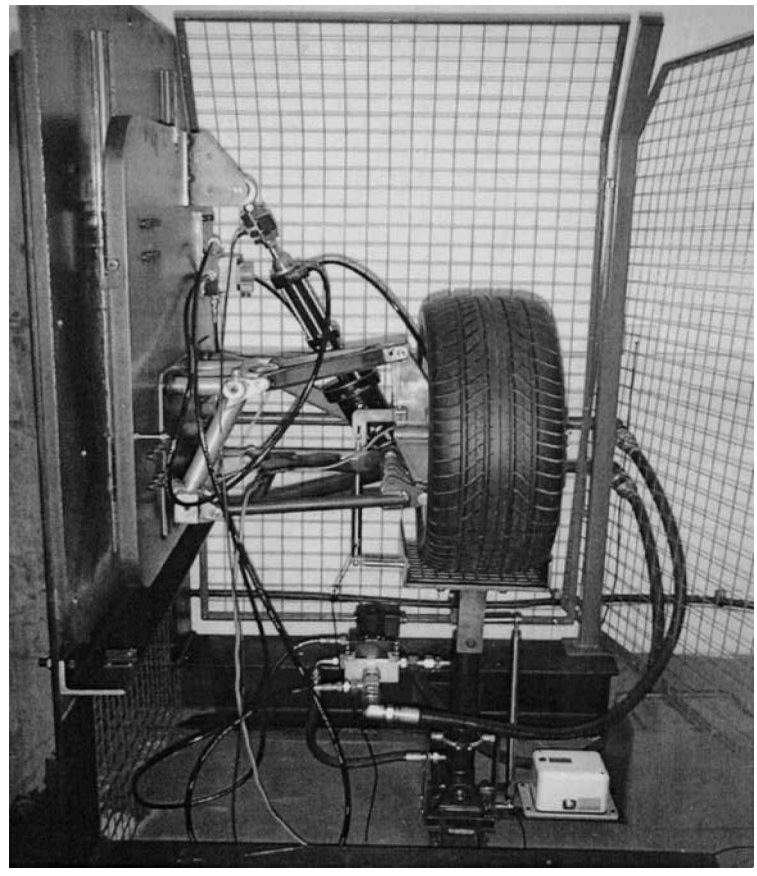

Fig. 1 Photograph of the quarter-vehicle test rig

appropriate, resulted in the following best estimates for the unknown parameters:

Effective bulk modulus
$\beta_e = 0.22 \times 10^9$ N/m^2
Cross-line leakage resistance
$R_i = 9.8 \times 10^{10}$ N/m^2/m^3 s

Oil stiffness
$k_o = (2\beta_e A^2/V) = 3.73 \times 10^5$ N/m
Tyre stiffness
$k_t = 2.8 \times 10^5$ N/m

Actuator viscous damping coefficient
$B_v = 300$ N/m s
Tyre damping coefficient
$B_t = 4000$ N/m s
Cross-line damping coefficient
$B_o = R_i A^2 = 5930$ N/m s

(1)

It will be deduced that the cross-line leakage damping is the most significant, followed by tyre damping and then the much lower pure viscous damping. Oil stiffness, even when corrected for actuator angle, is as significant as the tyre stiffness.

Figure 4a shows the amplitude response of the body, for a road input disturbance, and illustrates the two fundamental resonant frequencies of 3.9 and 20.2 Hz in the absence of damping. These frequencies may be easily verified from the Appendix, which produces the following undamped characteristic frequency equation:

$$1 - \left(\frac{M+m}{k_t} + \frac{M}{k_o \cos \alpha} \right) \omega^2 + \frac{Mm}{k_t k_o \cos \alpha} \omega^4 = 0 \tag{2}$$

It can be seen from (2) that the oil stiffness must be corrected for actuator angle. For an infinitely stiff actuator the single natural frequency would be 5 Hz, and for an infinitely stiff tyre the single natural frequency would be 5.9 Hz. Hence, for this system it is not a simple matter to couple stiffnesses and masses to define convenient 'body' or 'wheel' modes of oscillation. However, it is clear that the two natural frequencies appropriate to (2) are isolated by distinct body and wheel mass effects. Figure 4a shows that in reality the experimentally determined effects of actuator damping, B_v, and tyre damping, B_t, are evident, illustrating amplitude attenuation throughout the frequency range of interest. When cross-line leakage is introduced, and using the value experimentally identified from dynamic tests, the amplitude response is further, and significantly, changed as shown in Fig. 4b.

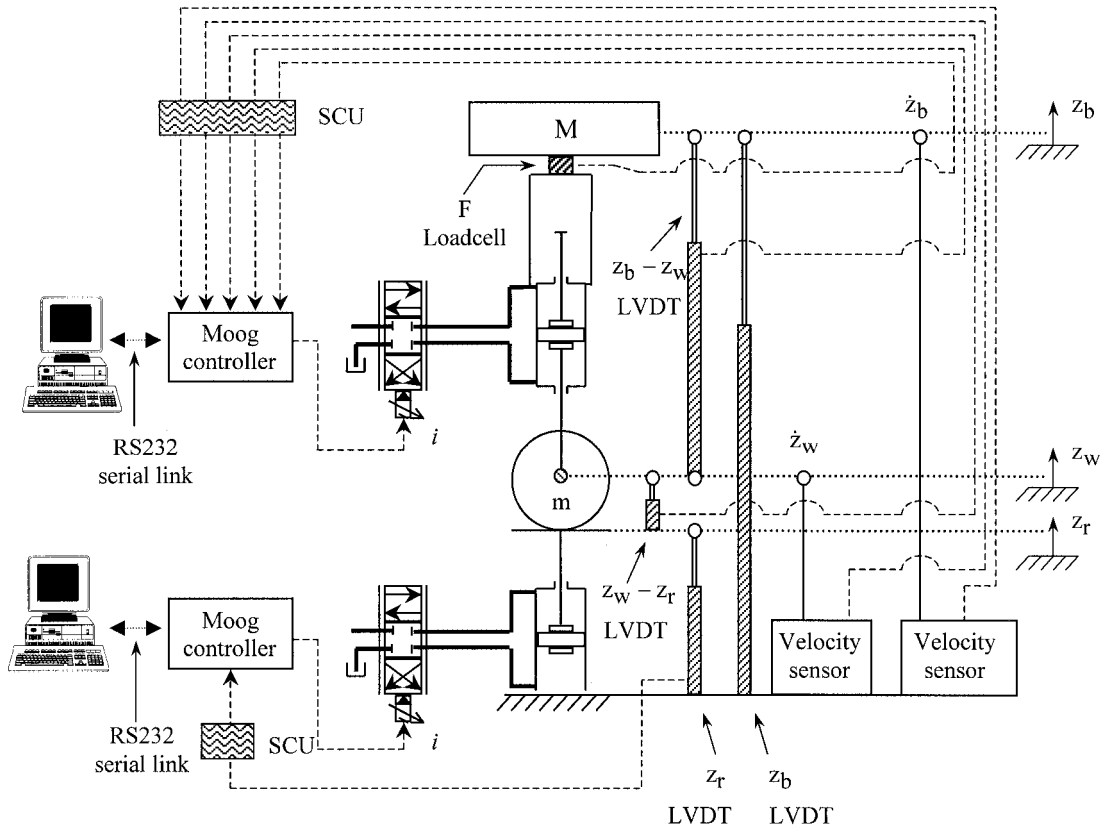

Fig. 2 Schematic of the measurement and control approach

3 SERVOVALVE NON-LINEAR GAIN SCHEDULING FOR ACTIVE CONTROL

For the range of movements presented in this study, extensive computer simulation studies, via the MATLAB environment, have been undertaken, assuming a critically lapped servovalve spool following experimental testing of the servovalve. A comparison with linearized transfer function approximations has verified that the linearized model is a sufficiently accurate representation of the dynamic behaviour. This is significantly aided in practice by the ability to compensate for the different servovalve flow gains when the active actuator is extending and retracting in real-time using the Moog M2000 programmable controller features. In the absence of cross-line leakage, the classical flow equations [**16**, **17**], as shown in the Appendix, result in the following ratio of retracting/extending steady state gains:

$$\frac{\text{Retracting gain}}{\text{Extending gain}} = \sqrt{\frac{P_s + P_L}{P_s - P_L}} \tag{3}$$

At a supply pressure of 200 bar and a load pressure differential of 108 bar, this ratio is 1.83, and it is a simple matter to utilize standard Moog M2000 controller functions ostensibly to remove this non-linear effect. In practice, the extending gain was increased by a factor of 1.3 and the retracting gain was decreased by the same factor, and this gave acceptably similar transient responses in each direction. The actual controller program used a comparator to sense the servovalve error signal sign, and then a parameter copier to change a variable gain function [**17**]. This is a highly significant feature of this study since a linearized transfer function approach may be used with more confidence for both parameter identification and closed-loop design. The effect of gain scheduling will be evident from the experimental results discussed later.

4 SYSTEM DYNAMICS MODELLING WITH ACTIVE CONTROL

Two issues arise when considering the system model, that is, servovalve cross-port leakage and active actuator piston seal leakage. Both components contribute to the total cross-line leakage resistance R_i as defined in this study. Measurements of the servovalve flow/current characteristic indicated that no significant spool overlap existed, but sufficiently accurate flow data could not be obtained around the zero current condition. A small cross-port leakage must exist at the null condition, and it is clear that pressure/flow damping must also occur in practice for the transient current condition. In addition, piston leakage must exist during dynamic operation even

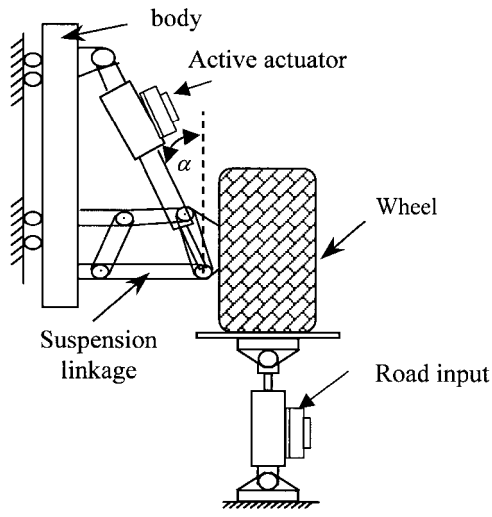

a) Schematic of the test rig

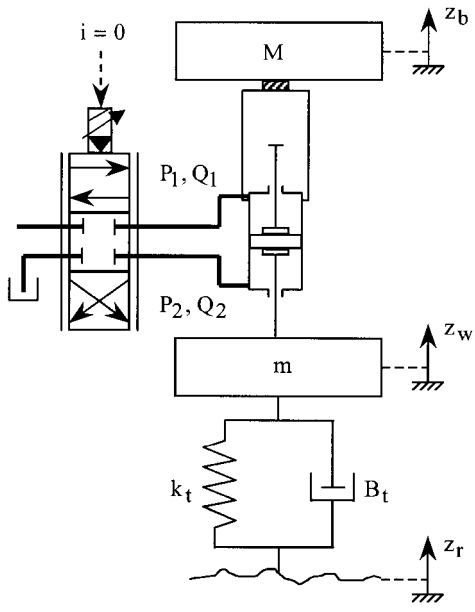

b) Schematic of the locked actuator

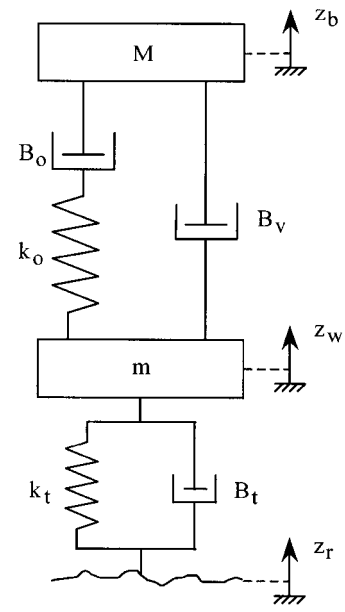

c) Dynamic model of the locked actuator

Fig. 3 Dynamic model with no active control

though the seal may well perform as required in the static mode.

The Lotus actuator had previously been extensively used by the company for in-house testing, although its exact condition could not be assessed. The complex dynamic leakage characteristic is difficult to quantify experimentally, particularly for short-stroke, fast-response actuators. It can be evaluated from frequency response tests by measuring the dynamic flowrates into and out of the actuator, together with the piston velocity and line pressures. Compressibility effects cannot be neglected, which means that this contribution must be numerically evaluated from the rate of change in each line pressure. In addition, for this test rig, the piston velocity must be numerically evaluated from the position measurement to allow the flow continuity equations to be used to evaluate the seal leakage. The parameter estimation aspect of this study showed that some form of cross-line damping must exist, given the recognized modelling approach adopted, and a single linear cross-line resistance, R_i, has been assumed to include a servovalve contribution and a piston seal leakage contribution. A first estimate of this cross-line leakage using the method previously described has indicated dynamic leakages of up to 3 l/min.

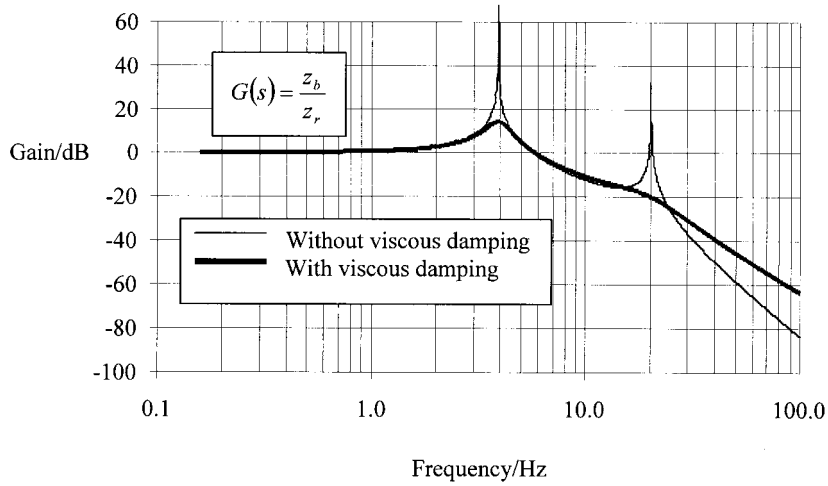

a) Neglecting cross-line leakage

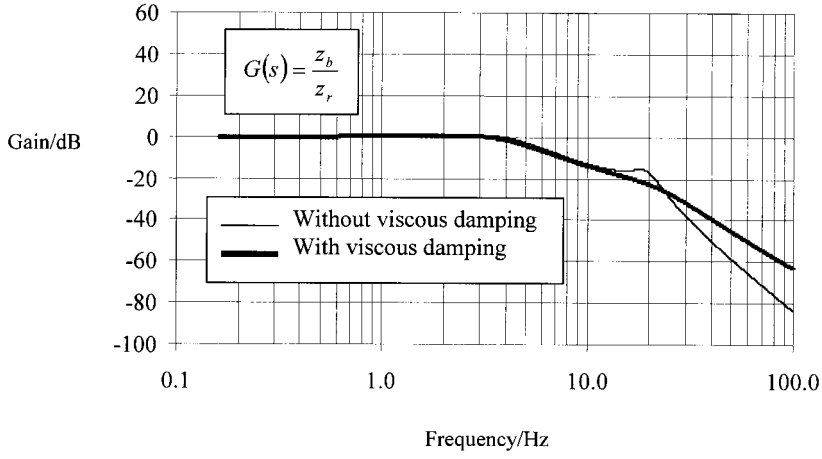

b) Including cross-line leakage

Fig. 4 Amplitude response of the vehicle body with active control switched off

4.1 Locked-actuator transfer function

As shown in the Appendix, the hydraulic force generated by the actuator is given by:

$$F=\frac{2k_i A}{sV/\beta_e+2/R_i}\,i-\frac{2A^2 s}{sV/\beta_e+2/R_i}\,(z_b-z_w) \qquad (4)$$

Therefore, with no feedback to the actuator, the second term on the right-hand side of equation (4) reflects the series oil stiffness and leakage damping terms shown in Fig. 3c. Considering the data, the locked-actuator configuration shown in Fig. 3b leads to the following transfer function:

$$\frac{z_b}{z_r}=\frac{b_0+b_1 s+b_2 s^2+b_3 s^3}{a_0+a_1 s+a_2 s^2+a_3 s^3+a_4 s^4+a_5 s^5} \qquad (5)$$

Transfer function (5), which represents no active control, is used for the amplitude responses shown in Fig. 4.

4.2 Effective bulk modulus

With respect to identification of the unknown parameters, it is necessary to determine the effective bulk modulus, particularly for this system with flexible hose lines. To determine the bulk modulus of the flexible hose, two approaches may be considered using both manufacturer's data and experimental measurements. For the test rig it was experimentally more expedient to use short flexible lines between the servovalve and actuator, and a synthetic material hose used in mobile applications was available. Data from the technical literature supplied by

the manufacturer [**18**] revealed a relatively poor material bulk modulus value of 0.2×10^9 N/m^2. This was confirmed by taking a transmission line measurement using fast acting flow meters at each end of a 12.2 m long flexible hose of the same material, with the input flowrate suddenly changed using a servovalve with a manual restrictor valve set to give a downstream load. The pure delay was measured to be 0.027 s, resulting in an effective bulk modulus of $\beta_e = 0.18 \times 10^9$ N/m^2, calculated using the simple wave propagation equation [**17**]. Hence, with Shell Tellus 37 mineral oil, having a working value bulk modulus of 1.4×10^9 N/m^2, this results in a bulk modulus of 0.21×10^9 N/m^2 for the hose only, which is in close agreement with the manufacturer's data. The combination of flexible hose and actuator chamber, taking the different volume into account, then results in an effective bulk modulus of 0.22×10^9 N/m^2 for the test rig. If the cylinder is not centrally positioned, then the effective bulk modulus for one side will vary between 0.18×10^9 N/m^2 and 0.27×10^9 N/m^2 as the volume of the cylinder chamber varies from zero to maximum. The combined effect of both sides of the actuator means that cylinder volume variation has a secondary effect on the effective bulk modulus.

4.3 Active actuator stiffness

Considering now the stiffness term on the right-hand side of equation (4), the dynamic transfer function becomes

$$\frac{\text{Dynamic stiffness}}{k_o} = \frac{s\tau}{(1+s\tau)},$$

$$\text{where } \tau = \frac{VR_i}{2\beta_e} \quad \text{and} \quad k_o = \frac{2\beta_e A^2}{V} \tag{6}$$

Inserting the data into (6) shows that the break frequency of this high-pass filter characteristic is 10 Hz, which means that the active actuator damping may only be considered as oil stiffness dominated above this frequency. Conversely, cross-line leakage effects occur below this break frequency. It would appear that typical load leakage flowrates of 1–3 l/min influence the dynamic transfer function of the test rig used in this study. Had rigid steel lines been used, the insertion of oil bulk modulus only would increase the break frequency from 10 to 63.6 Hz, thus creating a larger frequency range over which the cross-line leakage damping is dominant. The oil stiffness is increased by the same factor, thus also making it less significant when compared with cross-line damping. The net result is that the existing fluid bulk modulus characteristic only affects the amplitude characteristic shown in Fig. 4 for frequencies beyond 20 Hz and beyond the range of interest.

4.4 Wheel and tyre stiffness

A conventional machine static compression test was performed on the tyre and wheel, which produced a linear force/displacement characteristic plus a small hysteresis characteristic at typical tyre pressures. The stiffness was measured to be 1.4×10^5 N/m for diametral displacements of up to 40 mm. Therefore, an axle/ground stiffness of 2.8×10^5 N/m was assumed to be representative for the tyre when placed in its normal mode of static operation with a preloaded tyre pressure of 2.04 bar (30 lbf/in^2). The actual value used is confirmed later from the two-degree-of-freedom (2 DOF) experimental test.

5 MODEL VALIDATION VIA THE SINGLE-DEGREE-OF-FREEDOM (1 DOF) TEST

To determine the actuator viscous damping, B_v, and leakage resistance, R_i, it is necessary to introduce feedback control of the servovalve as shown in Fig 5. The simplest approach is to use position control of the actuator relative to the wheel with no ground motion. The programmable controller was used with an LVDT position transducer linked between the wheel axle and the body. For the expected frequency of oscillation of the vehicle body, the dynamics of the servovalve may be neglected. Therefore, the transfer function relating closed-loop body position, z_{bf}, to its desired value, z_{ref}, is given in the Appendix and takes the form

$$\frac{z_{bf}}{z_{ref}} = \frac{a_0}{a_0 + a_1 s + a_2 s^2 + a_3 s^3} \tag{7}$$

The coefficients of this third-order transfer function were identified using standard software tools within the MATLAB environment, the prediction error method producing the most stable approach from those available in the library. Experimental data, using step changes in demand for both extending and retracting, were obtained at a sampling frequency of 500 Hz, and the resulting discrete transfer function was transformed to continuous time using the bilinear transformation. This then allowed explicit determination of the unknown parameters, calculated to be

Actuator viscous damping coefficient
$B_v = 300$ N/m s

Actuator leakage coefficient
$R_i = 9.8 \times 10^{10}$ N/m^2/m^3 s

(8)

In addition, parameter identification from the 1 DOF test may be used to validate the servovalve flow gain derived in the Appendix. The identified value was found to be the mean of the extending and retracting gains and within 1 per cent of the value obtained from the servovalve no-load steady state flow test. This is logical since

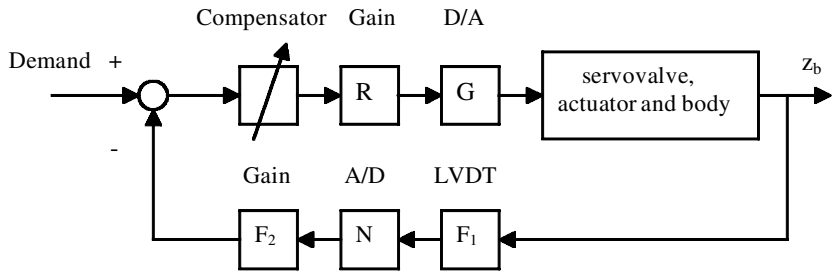

Fig. 5 Block diagram for the 1 DOF test

both actuator extending and retracting data were used for the parameter estimation procedure. The cross-line leakage resistance is lower than anticipated, although it will be recalled that it does contain terms due to servovalve and actuator piston seal leakage. Had the resistance been a factor of 4 greater, resulting in a leakage flowrate of 1.5 l/min under dynamic conditions, the break frequency given in (5) would decrease by the same factor to 2.5 Hz and would still influence system transient performance which has a damped natural frequency of typically 2 Hz.

A comparison between simulation and experiment is shown in Fig. 6, with gain scheduling being implemented in both cases. Demand changes of ± 6 mm are illustrated, and similar comparisons have been validated for a range of inputs.

6 MODEL VALIDATION VIA A 2 DOF TEST

To determine the tyre damping coefficient, B_t, and validate tyre stiffness, k_t, the road input, z_r, is used with servovalve control having a zero reference input but with negative feedback from the measured position $(z_b - z_w)$ for identification purposes only. Figure 7 shows the general block diagram including gain scheduling.

As shown in the Appendix, this results in a more complex transfer function relating body movement to road

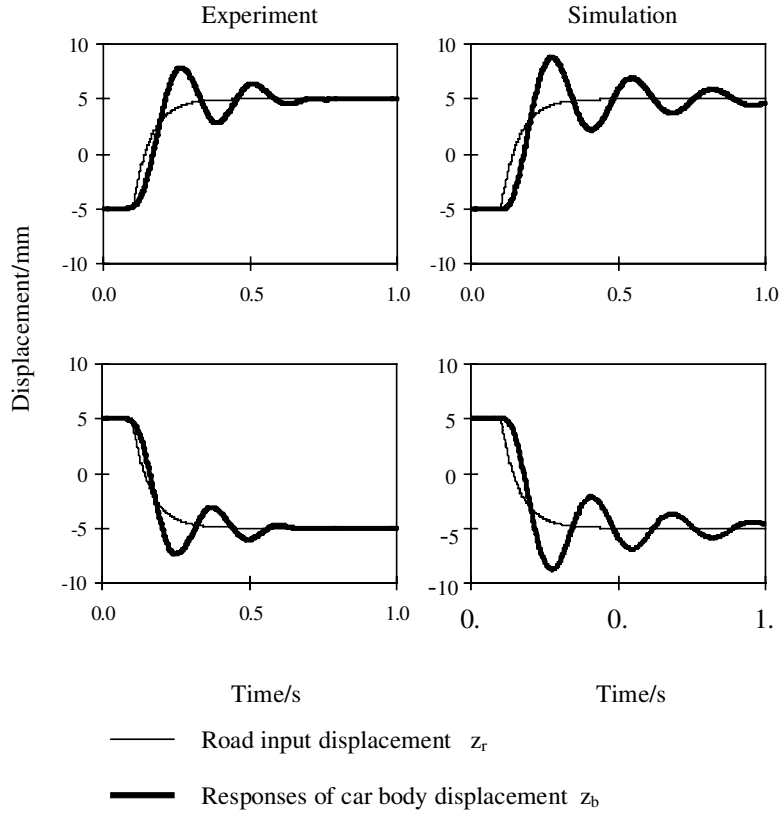

Fig. 6 Typical 1 DOF test result for B_v and R_i identification

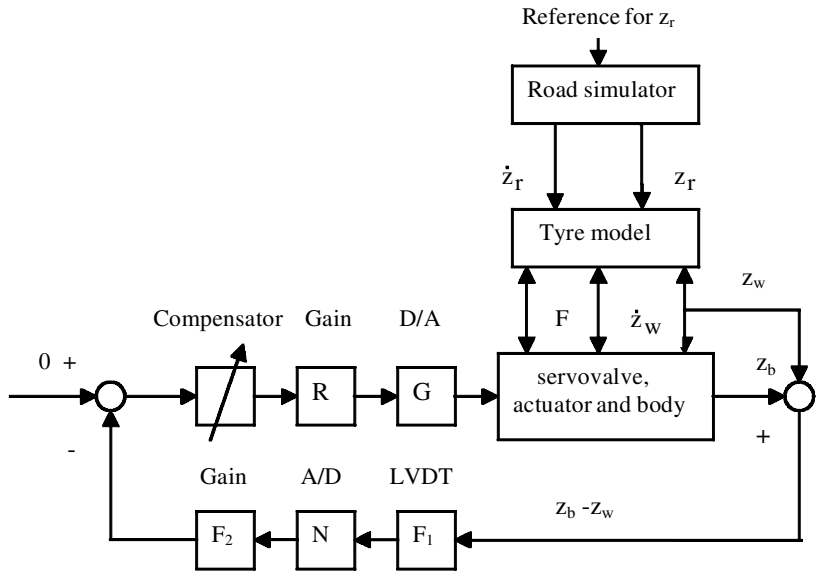

Fig. 7 Block diagram for the 2 DOF test

movement as follows:

$$\frac{z_b}{z_r} = \frac{b_0 + b_1 s + b_2 s^2 + b_3 s^3 + b_4 s^4}{a_0 + a_1 s + a_2 s^2 + a_3 s^3 + a_4 s^4 + a_5 s^5 + a_6 s^6} \quad (9)$$

Only two parameters need to be identified from this test, the tyre stiffness, k_t, and the tyre damping, B_v. These parameters were then varied to give the best fit between experimental step response data and transfer function (8) and resulted in the following:

Tyre stiffness $k_t = 2.8 \times 10^5$ N/m

Tyre velocity damping coefficient $B_t = 4000$ N/m s (10)

The tyre stiffness identified from dynamic testing is clearly a very accurate validation of the mean value deduced from static testing discussed previously.

It is important that the road input hydraulic response is correctly modelled to allow comparisons to be made

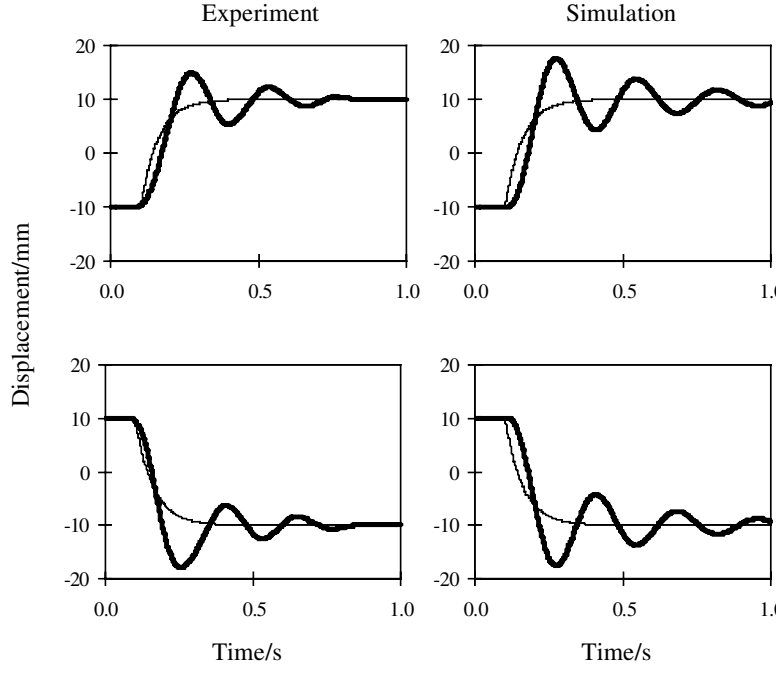

Fig. 8 2 DOF model validation for a road displacement input of ±10 mm

between experiment and theory, although a detailed mathematical knowledge of this separate position control loop is not necessary. A second programmable controller was used to close the position control loop, and it was deduced that a simple first-order transfer function, with a time constant of 0.06 s, was a sufficiently accurate representation of the dynamic behaviour over all the test conditions used. Comparisons between experiment and model prediction for the 2 DOF test, for step demand changes in road position, are shown in Fig 8.

Again, additional tests were used to validate the model for other input conditions. Generally, the results are good, the simulation predictions usually being a little more lightly damped than the experimental data.

7 PROPOSED OPEN-LOOP STATE-SPACE MODEL FOR THE ACTIVE SUSPENSION

Considering the described modelling, it is proposed that the most suitable state variables are:

(a) carbody velocity $\dot{z}_b$,
(b) wheel hub velocity $\dot{z}_w$,
(c) hydraulic force F,
(d) suspension displacement $z_b - z_w$,
(e) tyre deflection $z_w - z_r$.

Using the following state-space notation:

$$x_1 = \dot{z}_b$$
$$x_2 = \dot{z}_w$$
$$x_3 = F$$
$$x_4 = z_b - z_w$$
$$x_5 = z_2 - z_r$$

the open-loop equations may be written in the following state-space format:

$$\dot{x} = \mathbf{A}\boldsymbol{x} + \boldsymbol{B}e + \boldsymbol{G}_d\dot{z}_r$$

$$\boldsymbol{x} = \text{state vector} = \begin{bmatrix} \dot{z}_b \\ \dot{z}_w \\ F \\ z_b - z_w \\ z_w - z_r \end{bmatrix}$$

$\mathbf{A}$ = system matrix

$$= \begin{bmatrix} -\frac{B_v}{M} & \frac{B_v}{M} & \frac{\cos\alpha}{M} & 0 & 0 \\ \frac{B_v}{m} & -\frac{(B_v + B_t)}{m} & -\frac{\cos\alpha}{m} & 0 & -\frac{k_t}{m} \\ -\frac{2\beta_e A^2}{V} & \frac{2\beta_e A^2}{V} & -\frac{2\beta_e}{VR_i} & 0 & 0 \\ 1 & -1 & 0 & 0 & 0 \\ 0 & 1 & 0 & 0 & 0 \end{bmatrix}$$

$$\boldsymbol{B} = \text{input vector} = \begin{bmatrix} 0 \\ 0 \\ \frac{2k_1 AGP\beta_e}{V} \\ 0 \\ 0 \end{bmatrix}$$

$$\boldsymbol{G}_d = \text{disturbance vector} = \begin{bmatrix} 0 \\ \frac{B_t}{m} \\ 0 \\ 0 \\ -1 \end{bmatrix} \tag{11}$$

The control signal is e and $\dot{z}_r$ is the disturbance signal, i.e. the velocity of the road disturbance. For full state feedback, and considering the implementation of the Moog programmable controller, the control signal is given by

$$e = -\boldsymbol{K}\boldsymbol{x} = -N\boldsymbol{K}_1\mathbf{K}_2\boldsymbol{x}$$
$$e = -N[I_1 I_2 \dot{z}_b + J_1 J_2 \dot{z}_w + H_1 H_2 F + F_1 F_2 (z_b - z_w) + L_1 L_2 (z_w - z_r)] \tag{12}$$

where

$\boldsymbol{K}$ = 1 × 5 state feedback gain vector
N = A/D gain
$\boldsymbol{K}_1$ = 1 × 5 state feedback gain vector for the controller = $[I_1 \quad J_1 \quad H_1 \quad F_1 \quad L_1]$

$\mathbf{K}_2$ = 5 × 5 transducer gain matrix

$$\begin{bmatrix} I_2 & 0 & 0 & 0 & 0 \\ 0 & J_2 & 0 & 0 & 0 \\ 0 & 0 & H_2 & 0 & 0 \\ 0 & 0 & 0 & F_2 & 0 \\ 0 & 0 & 0 & 0 & L_2 \end{bmatrix} \tag{13}$$

Validation of the state-space model is indicated by Figs 9 and 10 which show measured and computed state variable responses for a step input to the servovalve controlling the road input system. The results represent non-optimized gains which were selected to give a stable behaviour, with feedback $z_b - z_w$ only being used. A range of input conditions from ±5 to ±15 mm have been validated, and indicate similar comparisons to those selected for Figs 9 and 10. The results show excellent directional symmetry owing to gain scheduling for both measured and simulated data, the simulation results indicating a small but detectable lower damping characteristic than the measured performance. The measured wheel hub velocity shows excessive damping compared

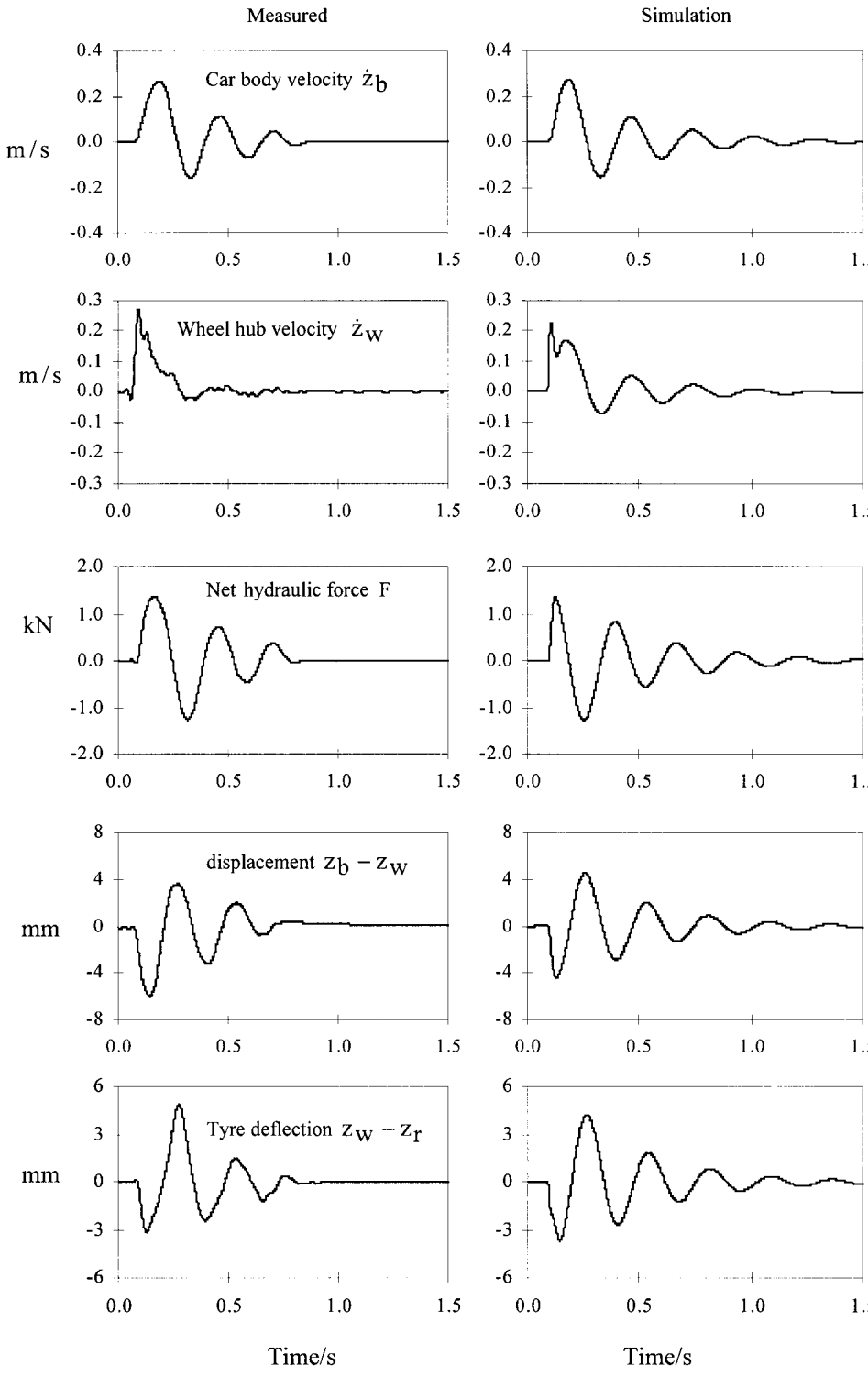

Fig. 9 Validation of the state variables for a −10 mm to +10 mm road step input

with the predicted response, although the unusual characteristic around the peak velocity is validated by the simulation. The measured data were obtained from a wire-wound d.c. tachogenerator, and it would appear that results are not reliable at speeds below 0.05 m/s.

8 CONCLUSIONS

1. All unknown system parameters may be deduced from two dynamic step response tests, referred to as a 1 DOF test and a 2 DOF test.

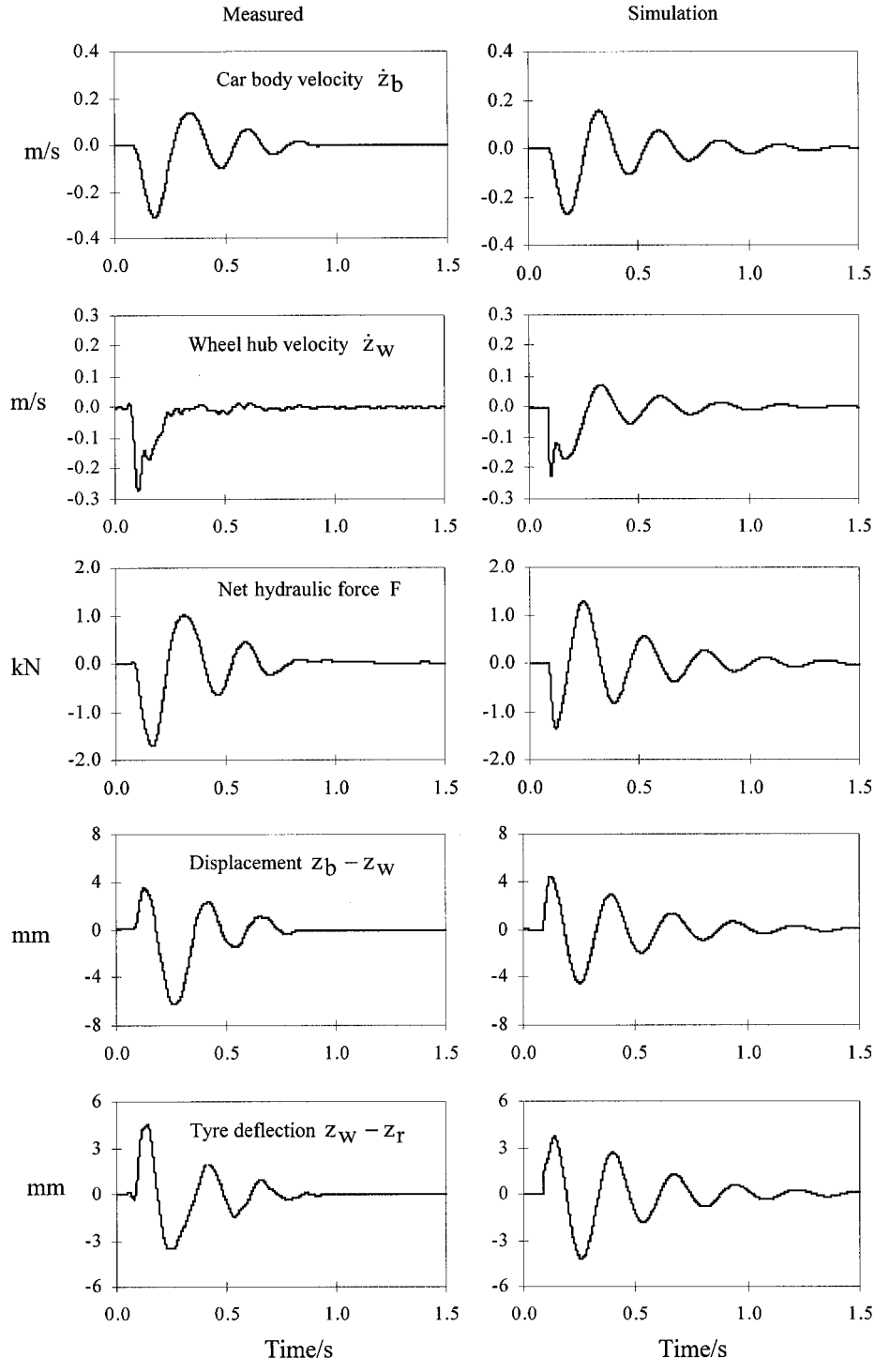

Fig. 10 Validation of the state variables for a +10 mm to −10 mm road step input

2. The overall velocity-dependent damping owing to viscous and coulomb friction was found to be negligible.
3. The presence of cross-line leakage was found to be as important as tyre damping, in the absence of active control, and this resulted in significant attenuation of the suspension response. Leakage could not be neglected for further modelling and control studies for this test configuration.
4. A further implication is that fixed gain control schemes may not be appropriate, as leakages change with wear or if replacement/refurbished actuators are used. The total cross-line leakage resistance was lower than expected, but it is clear from the modelling approach that an increase by a factor of 4 would still influence the suspension performance.
5. The presence of actuator leakage changes the actuator

dynamic force equation in two ways. Firstly, the relationship with applied current to the servovalve changes from an integral term to a first-order term. Secondly, the concept of static oil stiffness is not valid since the relationship between generated force and actuator displacement has a phase advance characteristic which exhibits a derivative behaviour at low frequencies. This high-pass filter characteristic is crucial to the performance of the suspension, and its effect is almost impossible to remove in practice, even for the smallest of leakages that can be achieved.

6. The low effective bulk modulus of the flexible lines resulted in an equivalent oil stiffness of similar order to the tyre stiffness. However, the dynamic contribution appears only to be significant for frequencies beyond 10 Hz even if rigid lines had been used. This is again associated with the actuator high-pass damping filter characteristic.
7. Parameter identification resulted in an accurate estimate of the servovalve mean flow gain using both extending and retracting experimental data. The application of this mean flow gain did give reasonable simulation predictions, but the use of experimental gain scheduling, based on the servovalve error signal, significantly improved the simulation validity of the linearized approach. The programmable controller approach gives more flexibility and allows fine tuning of the gain scheduling procedure significantly to reduce servovalve non-linear flow gain effects.
8. Further work is needed on the postulated dynamic leakage characteristic of the piston seal. This is conceptually possible, but preliminary work has shown that it requires accurate, synchronized, dynamic pressure, flowrate and velocity data together with accurate off-line numerical calculations.

REFERENCES

1 **Wright, P. G.** and **Williams, D. A.** The application of active suspension to high performance road vehicles. IMechE paper C239/84, 1984, pp. 23–28.
2 **Williams, P. G.,** *et al.* US Pat. 4625993, December 1986.
3 **Thompson, A. G.** and **Davis, B. R.** A technical note on the Lotus suspension patents. *Veh. Syst. Dynamics*, 1992, **20**, 381–383.
4 The Lotus active suspension system. Application Sheet 1, Lotus International, www.lotuseng.com.
5 **Sharp, R. S.** and **Crolla, D. A.** Road vehicle suspension system design—a review. *Veh. Syst. Dynamics*, 1987, **16**, 167–192.
6 **Appleyard, M.** and **Wellstead, P. E.** Active suspensions: some background. *IEE Proc. Control Theory Applic.*, 1995, **142**, 123–128.
7 **Elbeheiry, E. D.,** *et al.* Advanced ground vehicle suspension systems—a classified bibliography. *Veh. Syst. Dynamics*, 1995, **24**, 231–258.
8 **Hrovat, D.** Survey of advanced suspension developments and related optimal control applications. *Automatica*, 1997, **33**, 1781–1817.
9 **Mrad, R. B.,** *et al.* A nonlinear model of an automobile hydraulic active suspension. *ASME Advd Automn Technol.*, 1991, **DE Vol. 40**, 347–359.
10 **Engelmann, G. H.** and **Rizzoni, G.** Including the force generation process in active suspension control formulation. In Proceedings of American Control Conference, 1993, pp. 701–705.
11 **Rajamani, R.** and **Hedrick, J. K.** Performance of active automotive suspensions with hydraulic actuators: theory and experiment. In Proceedings of American Control Conference, 1994, pp. 1214–1218.
12 **Rajamani, R.** and **Hedrick, J. K.** Adaptive observers for active automative suspensions: theory and experiment. *IEEE Trans. Control Syst. Technol.*, 1995, **3**(1), 86–93.
13 **Thompson, A. G.** and **Chaplin, P. M.** Force control in electrohydraulic active suspensions. *Veh. Syst. Dynamics*, 1996, **25**, 185–202.
14 **Williams, R. A.** Automotive active suspensions. Part 1: basic principles. *Proc. Instn Mech. Engrs, Part D, Journal of Automobile Engineering*, 1997, **211**(D6), 415–426.
15 **Williams. R. A.** Automotive active suspensions. Part 2: practical considerations. *Proc. Instn Mech. Engrs, Part D, Journal of Automobile Engineering*, 1997, **211**(D6), 427–444.
16 **Watton, J.** *Fluid Power Systems*, 1989 (Prentice-Hall International).
17 **Surawattanawan, P.** The influence of hydraulic systems dynamics on the behaviour of a vehicle active suspension. PhD thesis, School of Engineering, Cardiff University, 2000.
18 *Synflex Hydraulic Hose Catalogue* (Eaton Corporation Engineered Polymer Products Division, Aurora, Ohio).

APPENDIX

System equations

Following experimental flow measurements on the servovalve [**17**], the non-linear servovalve flowrate equations are modelled as follows:

For $i \geqslant 0$ when extending:

$$Q_1 = k_f i \sqrt{|P_s - P_1|}\,\mathrm{sign}(P_s - P_1)$$

$$Q_2 = k_f i \sqrt{P_2}$$

For $i < 0$ when retracting:

$$Q_1 = k_f i \sqrt{P_1}$$

$$Q_2 = k_f i \sqrt{|P_s - P_2|}\,\mathrm{sign}(P_s - P_2)$$

It should be noted that Q_1 and Q_2 are negative values for the case $i < 0$. To obtain the equivalent linearized dynamic transfer functions for the system, note the steady state condition $i_0 = 0$, $P_1 = P_{10}$ and $P_2 = P_{20}$, and the flowrate equations become

$$Q_1 = Q_2 = k_i i$$

where the flow gain k_i is as follows:

$$k_f\sqrt{\frac{P_s-P_L}{2}} \qquad \text{when extending}$$

and

$$k_f\sqrt{\frac{P_s+P_L}{2}} \qquad \text{when retracting}$$

where

$$P_L = Mg/A$$

The actuator flowrate equations including compressibility and cross-line leakage effects may be written:

$$Q_1 = A(\dot{z}_b-\dot{z}_w)+\frac{V}{\beta_e}\dot{P}_1+\frac{(P_1-P_2)}{R_i}$$

$$Q_2 = A(\dot{z}_b-\dot{z}_w)-\frac{V}{\beta_e}\dot{P}_2+\frac{(P_1-P_2)}{R_i}$$

The actuator hydraulic force is given by

$$F = A(P_1-P_2)$$

The suspension equations of motion are

$$M\ddot{z}_b = F\cos\alpha - B_v(\dot{z}_b-\dot{z}_w)$$

$$m\ddot{z}_w = -F\cos\alpha + B_v(\dot{z}_b-\dot{z}_w)+k_t(z_r-z_w) + B_t(\dot{z}_r-\dot{z}_w)$$

Therefore, taking Laplace transforms and neglecting initial conditions allows the force transfer function to be written:

$$F = \frac{k_i A}{(sV/2\beta_e)+(1/R_i)}\,i - \frac{sA^2}{(sV/2\beta_e)+(1/R_i)}(z_b-z_w)$$

The locked actuator condition with no active feedback, $i=0$

$$F = -\frac{sA^2}{(sV/2\beta_e)+(1/R_i)}(z_b-z_w)$$

The transfer function relating road input, z_r, to carbody displacement, z_b, is

$$\frac{z_b}{z_r} = \frac{b_0+b_1s+b_2s^2+b_3s^3}{a_0+a_1s+a_2s^2+a_3s^3+a_4s^4+a_5s^5}$$

where the numerical coefficients are

$$a_0 = 6.51\times10^{-13}, \quad a_1 = 4.82\times10^{-14}$$

$$a_2 = 2.10\times10^{-15}, \quad a_3 = 3.48\times10^{-17}$$

$$a_4 = 2.37\times10^{-19}, \quad a_5 = 1.01\times10^{-21}$$

$$b_0 = 6.51\times10^{-13}, \quad b_1 = 2.02\times10^{-14}$$

$$b_2 = 1.64\times10^{-16}, \quad b_3 = 1.26\times10^{-19}$$

These terms are obtained from

$$a_0 = \frac{4k_t}{R_i}\left(A^2\cos\alpha+\frac{B_v}{R_i}\right)$$

$$a_1 = 2A^2\cos\alpha\left(\frac{k_tV}{\beta_e}+\frac{2B_t}{R_i}\right)+\frac{4B_v}{R_i}\left(\frac{k_TV}{\beta_e}+\frac{B_t}{R_i}\right)+\frac{4k_tM}{R_i^2}$$

$$a_2 = \frac{4m}{R_i}\left(A^2\cos\alpha+\frac{B_v}{R_i}\right)+\frac{B_vV}{\beta_e}\left(\frac{4B_t}{R_i}+\frac{k_tV}{\beta_e}\right)+\frac{4M}{R_i}\left(A^2\cos\alpha+\frac{B_v}{R_i}+\frac{k_tV}{\beta_e}+\frac{B_t}{R_i}\right)+\frac{2A^2B_tV\cos\alpha}{\beta_e}$$

$$a_3 = \frac{4m}{R_i}\left(\frac{B_vV}{\beta_e}+\frac{M}{R_i}\right)+\frac{MV}{\beta_e}\times\left(\frac{4B_v}{R_i}+\frac{2B_t}{R_i}+2A^2\cos\alpha+\frac{k_tV}{\beta_e}+\frac{2B_t}{R_i}\right)+\frac{B_tB_vV^2}{\beta_e^2}+\frac{2A^2mV\cos\alpha}{\beta_e}$$

$$a_4 = \frac{V}{\beta_e}\left(\frac{4mM}{R_i}+\frac{B_vmV}{\beta_e}+\frac{B_vMV}{\beta_e}+\frac{B_tMV}{\beta_e}\right)$$

$$a_5 = \frac{mMV^2}{\beta_e^2}$$

and

$$b_0 = \frac{4k_t}{R_i}\left(\frac{B_v}{R_i}+A^2\cos\alpha\right)$$

$$b_1 = \frac{4B_v}{R_i}\left(\frac{B_t}{R_i}+\frac{k_tV}{\beta_e}\right)+2A^2\cos\alpha\left(\frac{k_tV}{\beta_e}+\frac{2B_t}{R_i}\right)$$

$$b_2 = \frac{4B_tB_vV}{R_i\beta_e}+\frac{2A^2B_tV\cos\alpha}{\beta_e}+\frac{B_vk_tV^2}{\beta_e^2}$$

$$b_3 = \frac{B_tB_vV^2}{\beta_e^2}$$

1 DOF test

Assuming the position transducer gain F_1, an additional data acquisition gain N, the feedback gain F_2, the forward gain R, a D/A and servoamplifier gain G, then the

equations defining this test may be written:

$$2k_i Ai = 2A^2 \dot{z}_b + \frac{V}{\beta_e}\dot{F} + \frac{2}{R_i}F$$

$$M\ddot{z}_b = F\cos\alpha - B_v \dot{z}_b$$

$$i = G\,Re$$

$$e = z_{ref} - z_{bf}$$

$$z_{bf} = F_1 F_2 N z_b$$

The transfer function relating reference input z_{ref} to carbody displacement output (z_{bf} voltage equivalent) is

$$\frac{z_{bf}}{z_{ref}} = \frac{a_0}{a_0 + a_1 s + a_2 s^2 + a_3 s^3}$$

where the numerical coefficients are

$$a_0 = 2.30 \times 10^{-6}, \qquad a_1 = 1.14 \times 10^{-7}$$
$$a_2 = 5.00 \times 10^{-9}, \qquad a_3 = 7.78 \times 10^{-11}$$

These terms are obtained from

$$a_0 = 2AF_1F_2Gk_iNR\cos\alpha$$

$$a_1 = \left(\frac{2B_v}{R_i} + 2A^2\cos\alpha\right)$$

$$a_2 = \left(\frac{2M}{R_i} + \frac{B_v V}{\beta_e}\right)$$

$$a_3 = \frac{MV}{\beta_e}$$

2 DOF test

$$2k_i Ai = 2A^2(\dot{z}_b - \dot{z}_w) + \frac{V}{\beta_e}\dot{F} + \frac{2}{R_i}F$$

$$M\ddot{z}_b = F\cos\alpha - B_v(\dot{z}_b - \dot{z}_w)$$

$$m\ddot{z}_w = -F\cos\alpha + B_v(\dot{z}_b - \dot{z}_w) + k_t(z_r - z_w) + B_t(\dot{z}_r - \dot{z}_w)$$

$$i = GPe$$

$$e = 0 - NF_1F_2(z_b - z_w)$$

The transfer function relating road input, z_r, to carbody displacement, z_b, is

$$\frac{z_b}{z_r} = \frac{b_0 + b_1 s + b_2 s^2 + b_3 s^3 + b_4 s^4}{a_0 + a_1 s + a_2 s^2 + a_3 s^3 + a_4 s^4 + a_5 s^5 + a_6 s^6}$$

where the numerical coefficients are

$$a_0 = 2.80 \times 10^{-11}, \qquad a_1 = 1.50 \times 10^{-12},$$
$$a_2 = 8.25 \times 10^{-14}, \qquad a_3 = 2.55 \times 10^{-15},$$
$$a_4 = 3.48 \times 10^{-17}, \qquad a_5 = 2.37 \times 10^{-19},$$
$$a_6 = 1.01 \times 10^{-21}, \qquad b_0 = 2.80 \times 10^{-11},$$
$$b_1 = 1.50 \times 10^{-12}, \qquad b_2 = 2.65 \times 10^{-14},$$
$$b_3 = 1.64 \times 10^{-16}, \qquad b_4 = 1.26 \times 10^{-19}$$

These terms are obtained from

$$a_0 = \frac{4AGk_iNPF_1F_2k_t\cos\alpha}{R_i}$$

$$a_1 = 2AGk_iNP\left(\frac{F_1F_2k_tV\cos\alpha}{\beta_e} + \frac{2B_tF_1F_2\cos\alpha}{R_i}\right) + \frac{4k_t}{R_i}\left(A^2\cos\alpha + \frac{B_v}{R_i}\right)$$

$$a_2 = 2AGk_iNP\left(\frac{2F_1F_2m\cos\alpha}{R_i} + \frac{B_tF_1F_2V\cos\alpha}{\beta_e} + \frac{2F_1F_2M\cos\alpha}{R_i}\right) + 2A^2\cos\alpha\left(\frac{k_tV}{\beta_e} + \frac{2B_t}{R_i}\right) + \frac{4B_v}{R_i}\left(\frac{k_tV}{\beta_e} + \frac{B_t}{R_i}\right) + \frac{4k_tM}{R_i^2}$$

$$a_3 = 2AGk_iNP\left(\frac{F_1F_2mV\cos\alpha}{\beta_e} + \frac{F_1F_2MV\cos\alpha}{\beta_e}\right) + \frac{4m}{R_i}\left(A^2\cos\alpha + \frac{B_v}{R_i}\right) + \frac{B_vV}{\beta_e}\left(\frac{4B_t}{R_i} + \frac{k_tV}{\beta_e}\right) + \frac{4M}{R_i}\left(A^2\cos\alpha + \frac{B_v}{R_i} + \frac{k_tV}{\beta_e} + \frac{B_t}{R_i}\right) + \frac{2A^2B_tV\cos\alpha}{\beta_e}$$

$$a_4 = \frac{4m}{R_i}\left(\frac{B_vV}{\beta_e} + \frac{M}{R_i}\right) + \frac{MV}{\beta_e} \times \left(\frac{4B_v}{R_i} + \frac{2B_t}{R_i} + 2A^2\cos\alpha + \frac{k_tV}{\beta_e} + \frac{2B_t}{R_i}\right) + \frac{B_tB_vV^2}{\beta_e^2} + \frac{2A^2mV\cos\alpha}{\beta_e}$$

$$a_5 = \frac{V}{\beta_e}\left(\frac{4mM}{R_i} + \frac{B_vmV}{\beta_e} + \frac{B_vMV}{\beta_e} + \frac{B_tMV}{\beta_e}\right)$$

$$a_6 = \frac{mMV^2}{\beta_e^2}$$

$$b_0 = \frac{4AGk_iNPF_1F_2k_t\cos\alpha}{R_i}$$

$$b_1 = 2AGk_iNP\left(\frac{F_1F_2k_tV\cos\alpha}{\beta_e} + \frac{2B_tF_1F_2\cos\alpha}{R_i}\right) + \frac{4k_t}{R_i}\left(\frac{B_v}{R_i} + A^2\cos\alpha\right)$$

$$b_2 = 2AGk_iNP\left(\frac{B_tF_1F_2V\cos\alpha}{\beta_e}\right) + \frac{4B_v}{R_i}\left(\frac{B_t}{R_i} + \frac{k_tV}{\beta_e}\right) + 2A^2\cos\alpha\left(\frac{k_tV}{\beta_e} + \frac{2B_t}{R_i}\right)$$

$$b_3 = \frac{4B_tB_vV}{R_i\beta_e} + \frac{2A^2B_tV\cos\alpha}{\beta_e} + \frac{B_vk_tV^2}{\beta_e^2}$$

$$b_4 = \frac{B_tB_vV^2}{\beta_e^2}$$